SINTEF
PROCEEDINGS
1

Selected papers from 10th International Conference on Computational Fluid Dynamics in the Oil & Gas, Metallurgical and Process Industries

Progress in Applied CFD

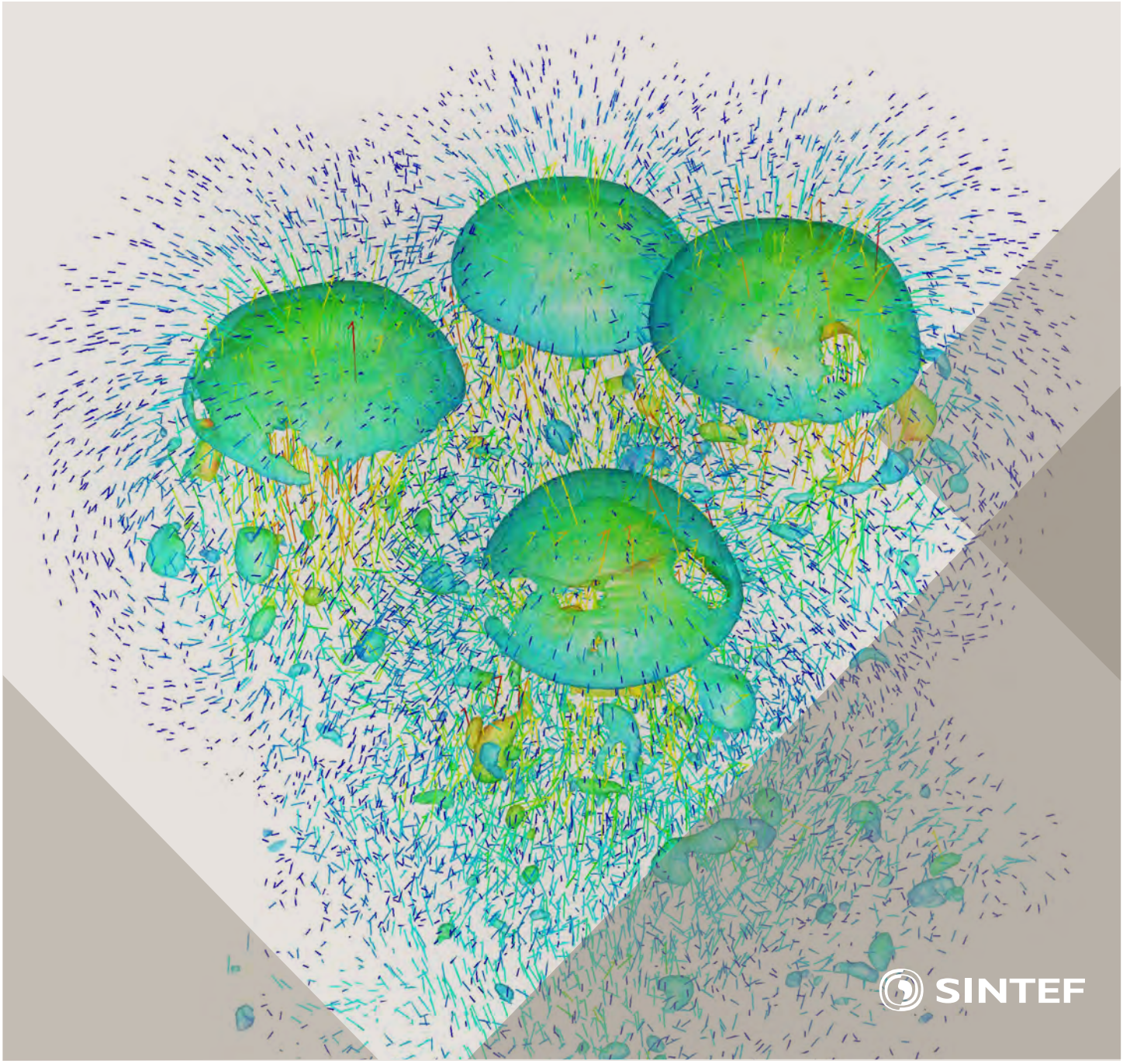

SINTEF Proceedings

Editors:
Jan Erik Olsen and Stein Tore Johansen

Progress in Applied CFD

Selected papers from 10th International Conference on Computational Fluid Dynamics in the Oil & Gas, Metallurgical and Process Industries

SINTEF Academic Press

SINTEF Proceedings no 1
Editors: Jan Erik Olsen and Stein Tore Johansen
Progress in Applied CFD
Selected papers from 10th International Conference on Computational Fluid Dynamics in the Oil & Gas, Metallurgical and Process Industries

Key words:
CFD, Flow, Modelling

Cover, illustration: Rising bubbles by Schalk Cloete

ISSN 2387-4287 (printed)
ISSN 2387-4295 (online)
ISBN 978-82-536-1432-8 (printed)
ISBN 978-82-536-1433-5 (pdf)

60 copies printed by AIT AS e-dit
Content: 100 g munken polar
Cover: 240 g trucard

SINTEF Academic Press
Address: Forskningsveien 3 B
PO Box 124 Blindern
N-0314 OSLO
Tel: +47 22 96 55 55
Fax: +47 22 96 55 08

www.sintef.no/byggforsk
www.sintefbok.no

SINTEF Proceedings
SINTEF Proceedings is a serial publication for peer-reviewed conference proceedings on a variety of scientific topics.
The processes of peer-reviewing of papers published in SINTEF Proceedings are administered by the conference organizers and proceedings editors. Detailed procedures will vary according to custom and practice in each scientific community.

PREFACE

This book contains selected papers from the 10th International Conference on Computational Fluid Dynamics in the Oil & Gas, Metallurgical and Process Industries. The conference was hosted by SINTEF in Trondheim in June 2014 and is also known as CFD2014 for short. The conference series was initiated by CSIRO and Phil Schwarz in 1997. So far the conference has been alternating between CSIRO in Melbourne and SINTEF in Trondheim. The conferences focus on the application of CFD in the oil and gas industries, metal production, mineral processing, power generation, chemicals and other process industries. The papers in the conference proceedings and this book demonstrate the current progress in applied CFD.

The conference papers undergo a review process involving two experts. Only papers accepted by the reviewers are presented in the conference proceedings. More than 100 papers were presented at the conference. Of these papers, 27 were chosen for this book and reviewed once more before being approved. These are well received papers fitting the scope of the book which has a slightly more focused scope than the conference. As many other good papers were presented at the conference, the interested reader is also encouraged to study the proceedings of the conference.

The organizing committee would like to thank everyone who has helped with paper review, those who promoted the conference and all authors who have submitted scientific contributions. We are also grateful for the support from the conference sponsors: FACE (the multiphase flow assurance centre), Total, ANSYS, CD-Adapco, Ascomp, Statoil and Elkem.

Stein Tore Johansen & Jan Erik Olsen

Organizing committee:

Conference chairman: Prof. Stein Tore Johansen
Conference coordinator: Dr. Jan Erik Olsen
Dr. Kristian Etienne Einarsrud
Dr. Shahriar Amini
Dr. Ernst Meese
Dr. Paal Skjetne
Dr. Martin Larsson
Dr. Peter Witt, CSIRO

Scientific committee:

J.A.M.Kuipers, TU Eindhoven
Olivier Simonin, IMFT/INP Toulouse
Akio Tomiyama, Kobe University
Sanjoy Banerjee, City College of New York
Phil Schwarz, CSIRO
Harald Laux, Osram
Josip Zoric, SINTEF
Jos Derksen, University of Aberdeen
Dieter Bothe, TU Darmstadt
Dmitry Eskin, Schlumberger
Djamel Lakehal, ASCOMP
Pär Jonsson, KTH
Ruben Shulkes, Statoil
Chris Thompson, Cranfield University
Jinghai Li, Chinese Academy of Science
Stefan Pirker, Johannes Kepler Univ.
Bernhard Müller, NTNU
Stein Tore Johansen, SINTEF
Markus Braun, ANSYS

CONTENTS

A BASELINE MODEL FOR MONODISPERSE BUBBLY FLOWS

Roland Rzehak[1*] , Eckhard Krepper[1] , Thomas Ziegenhein[1] , Dirk Lucas[1]

[1] Helmholtz-Zentrum Dresden - Rossendorf, P.O. Box 510119, 01314 Dresden, Germany

* E-mail: r.rzehak@hzdr.de

ABSTRACT

For practical applications the Euler-Euler two-fluid model relies on suitable closure relations describing interfacial exchange processes. The quest for models with a broad range of applicability allowing predictive simulations is an ongoing venture. A set of closure relations for adiabatic bubbly flow has been collected that represents the best available knowledge and may serve as a baseline for further improvements and extensions. In order to allow for predictive simulations the model must work for a certain range of applications without any adjustments. This is shown here for flows that allow to impose a fixed bubble size distribution which bypasses the need to model coalescence and breakup processes.

Keywords: Dispersed gas-liquid multiphase flow, Euler-Euler two-fluid model, closure relations, CFD simulation, model validation.

NOMENCLATURE

Greek Symbols

α	volume fraction [-]
ε	turbulent dissipation [$m^2\ s^{-3}$]
μ	viscosity [Pa s]
ρ	density [$kg\ m^{-3}$]
σ	surface tension [$N\ m^{-1}$]
τ	bubble-induced turbulence time scale [s]
ω	shear-induced turbulence time scale [s]

Latin Symbols

C	constant [-]
d	bubble diameter [m]
D	pipe / column diameter or width [m]
Eo	Eötvös number [-]
F	force [$N\ m^{-3}$]
g	gravitational constant [$m\ s^{-2}$]
J	superficial velocity [$m\ s^{-1}$]
k	turbulent kinetic energy [$m^2\ s^{-2}$]
ℓ	shear-induced turbulence length scale [m]
L	pipe / column length [m]
Mo	Morton number [-]
r	radial coordinate [m]
R	pipe / column radius or halfwidth [m]
Re	Reynolds number [-]
S	source term
u	axial component of mean velocity [$m\ s^{-1}$]
u'	axial component of fluctuating velocity [$m\ s^{-1}$]
y	coordinate normal to wall [m]

Sub/superscripts

B	bubble
eff	effective
G	gas
L	liquid
$turb$	turbulent
$\perp$	perpendicular to main motion

INTRODUCTION

CFD simulations of dispersed bubbly flow on the scale of technical equipment are feasible within the Eulerian two-fluid framework of interpenetrating continua. However, accurate numerical predictions rely on suitable closure models. A large body of work using different closure relations of varying degree of sophistication exists, but no complete, reliable, and robust formulation has been achieved so far.

An attempt has been made to collect the best available description for the aspects known to be relevant for adiabatic monodisperse bubbly flows (Rzehak and Krepper 2013), where closure is required for (i) the exchange of momentum between liquid and gas phases, and (ii) the effects of the dispersed bubbles on the turbulence of the liquid carrier phase. Apart from interest in its own right, results obtained for this restricted problem also provide a good starting point for the investigation of more complex situations including bubble coalescence and breakup, heat and mass transport, and possibly phase change or chemical reactions.

Predictive simulation requires a model that works without any adjustments within a certain domain of applicability. The purpose of the present contribution therefore is to validate this baseline model for a number of experimental data sets taken from the literature. These comprise flows in flat and round bubble columns as well as flows in vertical pipes of different diameter and length. A range of gas and liquid superficial velocities, gas volume fractions, and bubble sizes is covered. In all cases a fixed, but not necessarily

monodisperse distribution of bubble sizes is assumed as taken from the measurements.

The results show that reasonable agreement is obtained for all different data with the exact same model. This demonstration is the main new achievement that goes beyond previous individual consideration of some of the tests (Rzehak and Krepper 2013, Rzehak et al. 2013, Ziegenhein et al. 2013).

Restriction to situations where a fixed distribution of bubble sizes may be imposed excludes the additional complexity of modelling bubble coalescence and breakup processes and thus facilitates a step-by-step validation procedure. Expanding the range of applicability as well as the achieved accuracy is a continuously ongoing development effort.

DATA

Four test cases have been selected for the present investigation as described below. A summary of the setups is given in Table 1.

Table 1: Experimental conditions.

name	D mm	J_L m/s	J_G m/s	$\langle d_B \rangle$ mm	$\langle \alpha_G \rangle$ %
bin Mohd Akbar et al. (2012): flat bubble column					
A1	240	-	0.003	4.3	1.4
A2	240	-	0.013	5.5	6.2
Mudde et al. (2009): round bubble column					
M1	150	-	0.015	4.02	6.1
M2	150	-	0.017	4.06	7.6
M3	150	-	0.025	4.25	11
M4	150	-	0.032	4.47	16
M5	150	-	0.039	4.53	20
M6	150	-	0.049	4.44	25
Liu (1998): round pipe					
L21B	57.2	1.0	0.14	3.03	10.6
L21C	57.2	1.0	0.13	4.22	9.6
L22A	57.2	1.0	0.22	3.89	15.7
L11A	57.2	0.5	0.12	2.94	15.2
TOPFLOW: round pipe					
TL12-041	195.3	1.017	0.0096	4.99	1.1

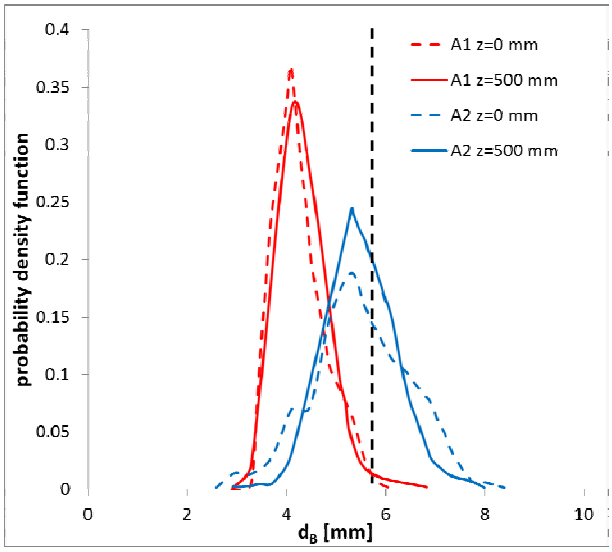

Figure 1: Measured bubble size distributions for tests A1 and A2.

Tests of bin Mohd Akbar et al. (2012)

The experiments of bin Mohd Akbar et al. (2012) were conducted in a flat bubble column of width D = 240 mm using air and water at ambient conditions. Without gas supply the water level was at 0.7 m. Profiles of gas volume fraction, axial liquid velocity, and axial turbulence intensity as well as the bubble size distribution were measured at a plane 0.5 m above the inlet. The bubble size distribution in addition was measured also near the inlet. As shown in Fig. 1 no significant change occurs over the column height. Two values of superficial gas velocities are available.

Tests of Mudde et al. (2009)

The setup of Mudde et al. (2009) consists of a round bubble column with diameter D = 150 mm again operated with air and water at ambient conditions. The ungassed fill-height was 1.3 m. Measurements of gas volume fraction and axial liquid velocity profiles were taken at different levels of which the one at 0.6 m above the inlet has been chosen for the comparison here. The sparger was designed specifically to provide highly uniform inlet conditions. Several values of the gas superficial velocity are available reaching rather large values of gas volume fraction. The mean bubble size and variation around it have been measured at two locations close to the inlet and close to the top water level. Since a slight increase is observed the average value of both measurements corresponding to the middle level has been used in the simulations.

Tests of Liu (1998)

The system studied by Liu (1998) is vertical upflow of water and air in a round pipe with inner diameter D = 57.2 mm, presumably at ambient conditions as well. The total length of the flow section was 3.43 m. A special gas injector was used that allowed to adjust the bubble size independently of liquid and gas superficial velocities. A variety of combinations of these three parameters are available. Radial profiles of void-fraction, mean bubble-size, axial liquid velocity, and axial liquid turbulence intensity were measured at an axial position $L / D = 60$ corresponding to fully developed conditions.

TOPFLOW tests

The TOPFLOW facility operated at HZDR has been specifically designed to obtain high quality data for the validation of CFD models. The tests used here (Lucas et al. 2010) have been run for cocurrent vertical upward flow of air and water in a round pipe with an inner diameter of D = 195.3 mm. Measurements were made by a wire mesh sensor at the top end of the pipe while gas injection occurs at different levels below. The operating conditions were set to a temperature of 30 °C and a pressure of 0.25 MPa at the location of the active gas injection. In this way the flow development can be studied as it would be observed for gas injection at a fixed position and measurements taken at different levels above. Distances L between the injection devices and the sensor are given in Table 2 for the different levels. The values of mean bubble size and average gas

Table 2: Length of test section for different levels of gas injection.

level		A	C	F	I	L	O	R
L	[mm]	221	335	608	1552	2595	4531	7802
L/D	[-]	1.1	1.7	3.1	7.9	13.3	23.2	39.9

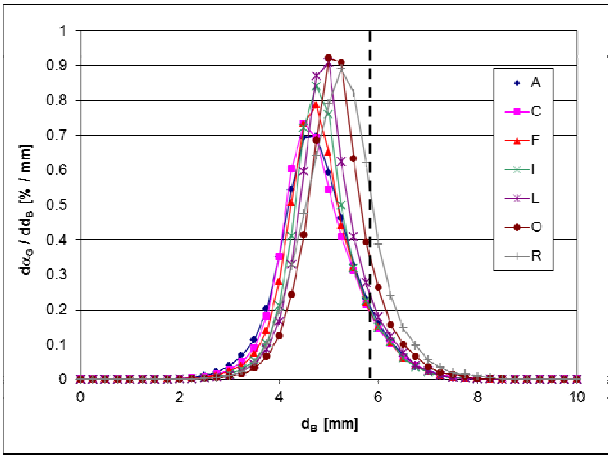

Figure 2: Distributions of bubble size for test TL12-041 at levels A to R.

volume fraction given in Table 1 correspond to the highest measurement level R.

Instrumentation with a wire mesh sensor allows collection of data on radial profiles of gas-fraction and gas-velocity as well as distributions of bubble size. A large range of liquid and gas superficial velocities was investigated in which all flow regimes from bubbly to annular occur. In the detailed report (Beyer et al. 2008) it has been noted that for bubbly flows the gas volume fluxes calculated from the measured profiles by integrating the product of volume fraction and velocity were systematically larger than those measured by the flow meter controlling the inlet. This deviation is likely to be caused by the distance between the sending and receiving wire planes, which leads to an increased value of void fraction, but a detailed explanation is not available yet. The ratio of the values calculated from the profiles (cf. Eq. (19)) to the values measured directly at the inlet has an approximately constant value of 1.2 over the bubbly flow regime (Beyer et al. 2008, Fig. 1-19). In the simulations the values measured by the flow meter will be used to set the inlet boundary condition. To get the same integral value of this conserved quantity for each cross-sectional plane, all measured void fractions are divided by 1.2 throughout this work.

A selection of tests in the bubbly flow regime has been made based on an examination of the measured bubble size distributions as shown in Fig. 2. It may be seen that a significant polydispersity is present as evidenced by a significant width of the measured bubble size distributions. The increase of average bubble size from level A to R is due to the decrease in hydrostatic pressure with height which in turn results in a proportionally decreasing gas density according to the ideal gas law. By transforming the distribution to the bubble mass as the independent variable this pressure effect may be eliminated. Apparently, for this test the opposing processes of bubble coalescence and -breakup are in a dynamic equilibrium where the net effect of both cancels. Therefore these processes need not be modeled explicitly, but the measured bubble mass distribution may be imposed in the simulations.

MODELING

The conservation equations of the Euler-Euler two-fluid model have been discussed at length in a number of books (e.g. Drew and Passman 1998, Yeoh and Tu 2010, Ishii and Hibiki 2011), while the extension to treat multiple bubble size and velocity classes (inhomogeneous MUSIG model) have been presented in research papers (e.g. Krepper et al. 2008). A broad consensus has been reached, so this general framework will not be repeated here.

Closure relations required to complete the model, in contrast, are still subject to considerable variation between researchers. Therefore, the specific correlations used here are given following (Rzehak and Krepper 2013) with the inclusion of a virtual mass force.

Bubble Forces

The closures used for the bubble forces are largely based on experiments on single bubbles in laminar flows. These are highly idealized conditions with respect to the applications intended to cover by Euler-Euler simulations, i.e. turbulent flows with void fractions up to ~25%. Nevertheless as will be shown, useful results may be obtained with this approach although improvements are obviously desirable.

Drag Force

The drag force reflects the resistance opposing bubble motion relative to the surrounding liquid. The corresponding gas-phase momentum source is given by

$$\mathbf{F}^{drag} = -\frac{3}{4d_B} C_D \rho_L \alpha_G |\mathbf{u}_G - \mathbf{u}_L| \, (\mathbf{u}_G - \mathbf{u}_L) \,. \quad (1)$$

The drag coefficient C_D depends strongly on the Reynolds number and for deformable bubbles also on the Eötvös number, but turns out to be independent of Morton number. A correlation distinguishing different shape regimes has been suggested by Ishii and Zuber (1979), namely

$$C_D = \max\left(C_{D,sphere}, \min\left(C_{D,ellipse}, C_{D,cap}\right)\right), \quad (2)$$

where

$$C_{D,sphere} = \frac{24}{\mathrm{Re}}\left(1 + 0.1\ \mathrm{Re}^{0.75}\right)$$
$$C_{D,ellipse} = \frac{2}{3}\sqrt{\mathrm{Eo}} \quad . \quad (3)$$
$$C_{D,cap} = \frac{8}{3}$$

This correlation was compared with an extensive data set on the terminal velocity of bubbles rising in quiescent liquids covering several orders of magnitude for each of *Re*, *Eo* and *Mo* in (Tomiyama et al. 1998) with good agreement except at high values of *Eo*.

Lift Force

A bubble moving in an unbounded shear flow experiences a force perpendicular to the direction of its motion. The momentum source corresponding to this shear lift force, often simply referred to as lift force, can be calculated as (Zun 1980):

$$\mathbf{F}^{lift} = -C_L \rho_L \alpha_G (\mathbf{u}_G - \mathbf{u}_L) \times rot(\mathbf{u}_L) \,. \qquad (4)$$

For a spherical bubble the shear lift coefficient C_L is positive so that the lift force acts in the direction of decreasing liquid velocity, i.e. in case of co-current pipe flow in the direction towards the pipe wall. Experimental (Tomiyama et al. 2002) and numerical (Schmidtke 2008) investigations showed, that the direction of the lift force changes its sign if a substantial deformation of the bubble occurs. From the observation of the trajectories of single air bubbles rising in simple shear flow of a glycerol water solution the following correlation for the lift coefficient was derived:

$$C_L = \begin{cases} \min[0.288 \tanh(0.121 \mathrm{Re}), f(Eo_\perp)] & Eo_\perp < 4 \\ f(Eo_\perp) & for \quad 4 < Eo_\perp < 10 \\ -0.27 & 10 < Eo_\perp \end{cases}$$

with (5)

$$f(Eo_\perp) = 0.00105 Eo_\perp^3 - 0.0159 Eo_\perp^2 - 0.0204 Eo_\perp + 0.474 \,.$$

This coefficient depends on the modified Eötvös number given by

$$Eo_\perp = \frac{g(\rho_L - \rho_G) d_\perp^2}{\sigma} \,, \qquad (6)$$

where $d_\perp$ is the maximum horizontal dimension of the bubble. It is calculated using an empirical correlation for the aspect ratio by Wellek et al. (1966) with the following equation:

$$d_\perp = d_B \sqrt[3]{1 + 0.163 \; Eo^{0.757}} \,, \qquad (7)$$

where *Eo* is the usual Eötvös number.

The experimental conditions on which Eq. (5) is based, were limited to the range $-5.5 \le log_{10} Mo \le -2.8$, $1.39 \le Eo \le 5.74$ and values of the Reynolds number based on bubble diameter and shear rate $0 \le Re \le 10$. The water-air system at normal conditions has a Morton number $Mo = 2.63e\text{-}11$ which is quite different, but good results have nevertheless been reported for this case (Lucas and Tomiyama 2011).

For the water-air system the sign change of C_L occurs at a bubble diameter of $d_B = 5.8$ *mm.*

Wall Force

A bubble translating next to a wall in an otherwise quiescent liquid also experiences a lift force. This wall lift force, often simply referred to as wall force, has the general form

$$\mathbf{F}^{wall} = \frac{2}{d_B} C_W \rho_L \alpha_G |\mathbf{u}_G - \mathbf{u}_L|^2 \hat{\mathbf{y}} \,, \qquad (8)$$

where $\hat{\mathbf{y}}$ is the unit normal perpendicular to the wall pointing into the fluid. The dimensionless wall force coefficient C_W depends on the distance to the wall *y* and is expected to be positive so the bubble is driven away from the wall.

Based on the observation of single bubble trajectories in simple shear flow of a glycerol water solution Tomiyama et al. (1995) and later Hosokawa et al. (2002) concluded a different functional dependence

$$C_W(y) = f(Eo) \left(\frac{d_B}{2y} \right)^2 \,. \qquad (9)$$

In the limit of small Morton number the correlation

$$f(Eo) = 0.0217 \;\; Eo \qquad (10)$$

can be derived from the data of Hosokawa et al. (2002). The experimental conditions on which Eq. (10) is based are $2.2 \le Eo \le 22$ and log10 Mo = -2.5 … -6.0 which is still different from the water-air system with Mo = 2.63e-11, but a recent investigation (Rzehak et al. 2012) has nonetheless shown that good predictions are obtained also for air bubbles in water.

Turbulent Dispersion Force

The turbulent dispersion force describes the effect of the turbulent fluctuations of liquid velocity on the bubbles. Burns et al. (2004) derived an explicit expression by Favre averaging the drag force as:

$$\mathbf{F}^{disp} = -\frac{3}{4} C_D \frac{\alpha_G}{d_B} |\mathbf{u}_G - \mathbf{u}_L| \frac{\mu_L^{turb}}{\sigma_{TD}} \left(\frac{1}{\alpha_L} + \frac{1}{\alpha_G} \right) \mathrm{grad}\, \alpha_G \,. \qquad (11)$$

In analogy to molecular diffusion, σ_{TD} is referred to as a Schmidt number. In principle it should be possible to obtain its value from single bubble experiments also for this force by evaluating the statistics of bubble trajectories in well characterized turbulent flows, but to our knowledge this has not been done yet. A value of $\sigma_{TD} = 0.9$ is typically used.

In the same work the expression for the so-called Favre averaged drag (FAD) model has also been compared with other suggestions from the literature and it was shown that all agree at least in the limit of low void fraction.

Virtual Mass Force

When a bubble is accelerated, a certain amount of liquid has to be set into motion as well. This may be expressed as a force acting on the bubble as

$$\mathbf{F}^{VM} = -C_{VM} \rho_L \alpha_G \left(\frac{D_G \mathbf{u}_G}{Dt} - \frac{D_L \mathbf{u}_L}{Dt} \right), \qquad (12)$$

where D_G / Dt and D_L / Dt denote material derivatives with respect to the velocity of the indicated phase. For the virtual mass coefficient a value of 0.5 has been derived for isolated spherical bubbles in both inviscid and creeping flows by Auton et al. (1988) and Maxey and Riley (1983), respectively. Results of direct simulations of a single bubble by Magnaudet et al. (1995) suggest that this value also holds for intermediate values of *Re*. For steady parallel flows this force vanishes and can be excluded from the calculations**.**

Bubble-induced Turbulence

Due to the low density and small spatial scales of the dispersed gas it suffices to consider turbulence only in the

continuous liquid phase. We adopt a two equation turbulence model for the liquid phase with additional source terms describing bubble induced turbulence. The formulation given is equally applicable to either k-ε, k-ω or SST model, but the latter (Menter 2009) will be used presently.

Concerning the source term describing bubble effects in the k-equation there is large agreement in the literature. A plausible approximation is provided by the assumption that all energy lost by the bubble due to drag is converted to turbulent kinetic energy in the wake of the bubble. Hence, the k-source becomes

$$S_L^k = \mathbf{F}_L^{drag} \cdot (\mathbf{u}_G - \mathbf{u}_L). \quad (13)$$

For the ε-source a similar heuristic is used as for the single phase model, namely the k-source is divided by some time scale τ so that

$$S_L^\varepsilon = C_{\varepsilon B} \frac{S_L^k}{\tau}. \quad (14)$$

Further modeling then focuses on the time scale τ proceeding largely based on dimensional analysis. This follows the same line as the standard modeling of shear-induced turbulence in single phase flows (Wilcox 1998), where production terms in the ε-equation are obtained by multiplying corresponding terms in the k-equation by an appropriate time scale which represents the life-time of a turbulent eddy before it breaks up into smaller structures. In single phase turbulence the relevant variables are obviously k and ε from which only a single time scale $\tau = k_L / \varepsilon_L$ can be formed. For the bubble-induced turbulence in two-phase flows the situation is more complex. There are now two length and two velocity scales in the problem, where one of each is related to the bubble and the other to the turbulent eddies. From these a total of four different time scales can be formed. In the absence of theoretical arguments to decide which of these is the most relevant one, a comparison of all four alternatives (Rzehak and Krepper 2013, 2013a) has shown the best performance for the choice

$$\tau = \frac{d_B}{\sqrt{k_L}}. \quad (15)$$

For the coefficient $C_{\varepsilon B}$ a value of 1.0 to was found to give reasonable results.

For use with the SST model, the ε-source is transformed to an equivalent ω-source which gives

$$S_L^\omega = \frac{1}{C_\mu k_L} S_L^\varepsilon - \frac{\omega_L}{k_L} S_L^k \quad . \quad (16)$$

This ω-source is used independently of the blending function in the SST model since it should be effective throughout the fluid domain.

Since bubble-induced effects are included in k and ε / ω due to the respective source terms, the turbulent viscosity is evaluated from the standard formula

$$\mu_L^{turb} = C_\mu \rho_L \frac{k_L^{\,2}}{\varepsilon_L} \quad (17)$$

and the effective viscosity is simply

$$\mu_L^{eff} = \mu_L^{mol} + \mu_L^{turb}. \quad (18)$$

Boundary conditions on k and ε / ω are taken the same as for single phase flow, which is consistent with the view that the full wall shear stress is exerted by the liquid phase which contacts the full wall area. A single phase wall function is employed to avoid the need to resolve the viscous sublayer.

All turbulence model parameters take their usual single phase values.

RESULTS

Simulations were performed by a customized version of ANSYS CFX. Depending on the test under investigation different setups were used as listed in Table 3. The calculations were made either in stationary mode imposing plane / axisymmetric conditions by considering only a thin slice / sector of the domain together with symmetry conditions or in transient mode with subsequent averaging of the results and fully 3D on the same domain as the experiments. The reason to choose the stationary or quasi-2D approximation whenever applicable is that it drastically reduces the computation time. For the transient simulations the reported quantities are averages over the statistically steady state.

At the inlet a uniform distribution of gas throughout the cross-section was assumed or the injection nozzles or needles were modelled as CFX point sources. For the liquid, fully developed single phase velocity and turbulence profiles were assumed in the pipe flow cases.

At the top a pressure boundary condition was set for the pipe flow cases while the CFX degassing condition was employed for the bubble column cases. On the walls a no-slip condition was used for the liquid phase and a free-slip condition for the gas phase assuming that direct contacts between the bubbles and the walls are negligible. To avoid the need to resolve the viscous sublayer, the automatic wall function treatment of CFX was applied.

Concerning bubble size a monodisperse approximation was used whenever the bubbles are smaller than the critical diameter of 5.8 mm where the lift force changes its sign. In the other cases an inhomogeneous MUSIG model with two velocity groups corresponding to bubbles smaller and larger than 5.8 mm was applied.

Table 3: Simulation setup summary.

tests	domain	solution	MUSIG size groups	MUSIG velocity groups	inlet
bin Mohd Akbar et al. (2012): flat bubble column					
A1	3D	transient	1	1	needles
A2	3D	transient	2	2	needles
Mudde et al. (2009): round bubble column					
M1	3D	transient	1	1	uniform
M2	3D	transient	1	1	uniform
M3	3D	transient	1	1	uniform
M4	3D	transient	1	1	uniform
M5	3D	transient	1	1	uniform
M6	3D	transient	1	1	uniform
Liu (1998): round pipe					
L21B	2D sector	stationary	1	1	uniform
L21C	2D sector	stationary	1	1	uniform
L22A	2D sector	stationary	1	1	uniform
L11A	2D sector	stationary	1	1	uniform
TOPFLOW: round pipe					
TL12-041	3D	stationary	10	2	nozzles

If there is a significant variation of pressure within the domain, the gas density will change according to the ideal gas law and consequently the bubble size changes since mass is conserved. Yet the flow of both gas and liquid remains incompressible to a good approximation. To keep the computational advantage of treating both gas and liquid as incompressible fluids with constant material properties in a fully developed flow, as discussed in Rzehak et al. (2012), the gas flux at the inlet is adjusted to the value obtained by evaluating

$$J_G = 2\pi \int_0^{D/2} \alpha_G(r)\, u_G(r)\; r\, dr \qquad (19)$$

using the data at the measurement location. In cases where only $\mathbf{u}_L$ but not $\mathbf{u}_G$ has been measured, an estimate of the latter may be obtained from the former and α_G based on the assumption of fully developed stationary flow. Where this procedure has been applied the adjusted values are given in Table 1.

Turbulence data frequently give the axial intensity of turbulent fluctuations while in the simulations based on two-equation models only the turbulent kinetic energy is available. For a comparison it has to be considered that wall-bounded turbulence is anisotropic with the axial component of fluctuating velocity being larger than those in radial and azimuthal directions. The ratio $\sqrt{k}$ / *u'* is bounded between $\sqrt{(1/2)} \approx 0.71$ and $\sqrt{(3/2)} \approx 1.22$ corresponding to unidirectional and isotropic limiting cases. Taking *u'* as an estimate for $\sqrt{k}$ thus provides an estimate that is accurate to within ~20%.

Tests of bin Mohd Akbar et al. (2012)

For the tests of bin Mohd Akbar et al. (2012) transient 3D simulations were performed using a gas inlet configuration that represents the experimental needle sparger. Due to the small column height the pressure effect is negligible. For the lower value of gas volume flux a monodisperse bubble size distribution was imposed, for the higher value two MUSIG size and velocity groups were used with diameters of 5.3 mm and 6.3 mm and relative amounts of 63 % and 37 %. For the evaluation of *k*, the axial component of the resolved transient fluctuations has been added to the unresolved part obtained from the turbulence model.

A comparison between simulation results and measured data is shown in Fig. 3. As may be seen the agreement between both is quite good for gas volume fraction and axial liquid velocity. Slight differences are that the predicted gas volume fraction profile is a little bit too peaked near the wall and there is a small dip in the predicted liquid velocity in the center of the column. The turbulent kinetic energy in the column center is somewhat underpredicted by the simulations and the peak in *k* near the wall is not reproduced by the simulations.

Tests of Mudde et al. (2009)

For the tests of Mudde et al. (2009), transient 3D simulations were performed assuming a uniform distribution of gas at the inlet. For the column height of 1.3 m the pressure effect is still small enough to be neglected. A monodisperse bubble size distribution corresponding to the measured values was used.

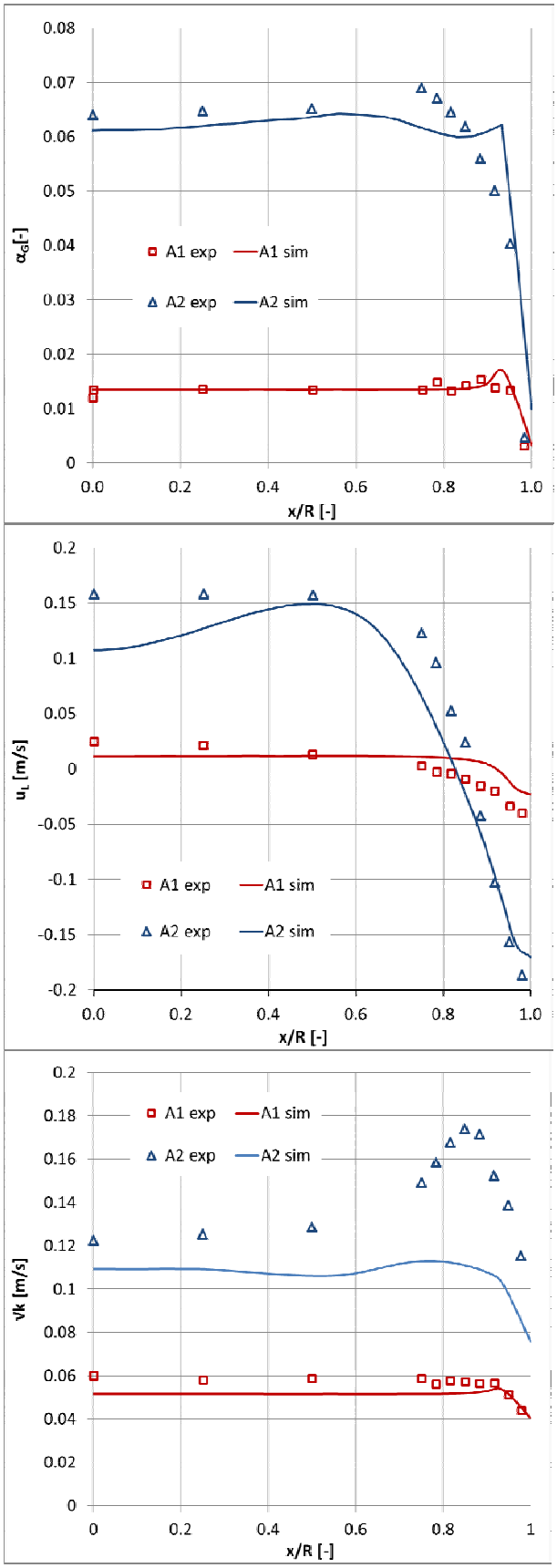

Figure 3: Gas volume fraction (top), axial liquid velocity (middle), and turbulent kinetic energy (bottom) for the tests of bin Mohd Akbar et al. (2012). Solid lines: simulation results, symbols: measured values. Only half of the column is shown.

Measured and calculated values are compared in Fig. 4. Clearly the gas volume fractions are predicted within the experimental errors. The calculated liquid velocity profiles do not depend on the total gas hold-up. Since the measured profiles do not show any systematic trend as a function of this variable, their variation is most likely an indication of the measurement errors.

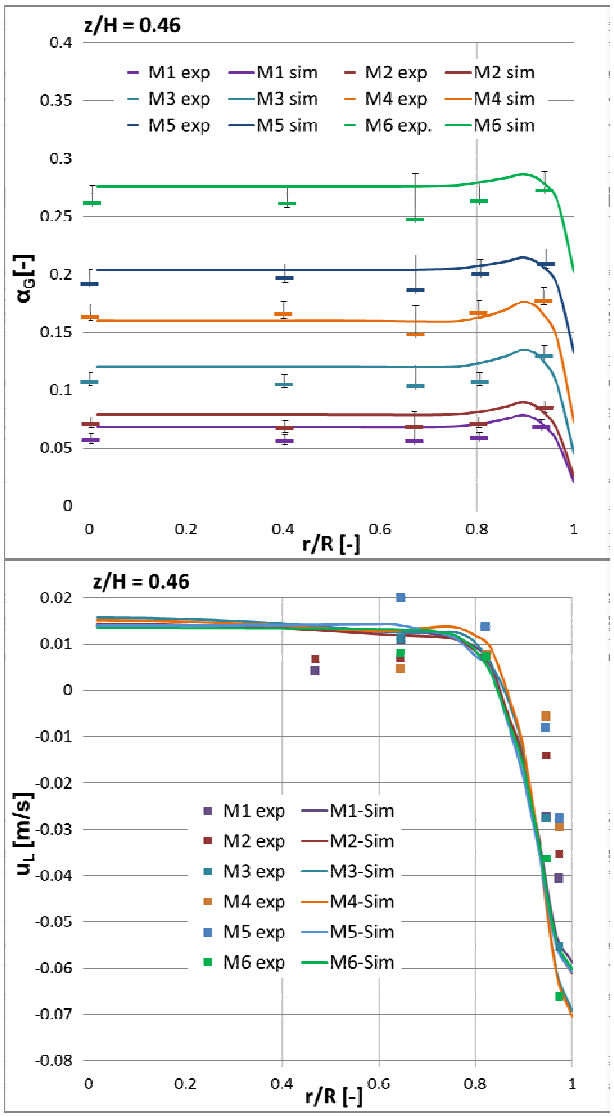

Figure 4: Gas volume fraction (top) and axial liquid velocity (bottom) for the tests of Mudde et al. (2009). Solid lines: simulation results, symbols: measured values.

Tests of Liu (1998)

For the tests of Liu (1998) stationary axisymmetric simulations were done assuming a uniform distribution of gas at the inlet. Since the pressure effect is significant for the 3.43 m long pipe, gas volume fluxes were adjusted to allow treating the gas as incompressible. A monodisperse bubble size distribution was imposed with the bubble size set equal to the average of the measured profiles.

The comparison of calculated and measured profiles in Fig. 5 shows reasonable agreement for the gas volume fraction and the axial liquid velocity. Notable deviations occur in the region close to the wall where the simulations predict the peak in the gas fraction too high and the gradient of the liquid velocity too steep. For the

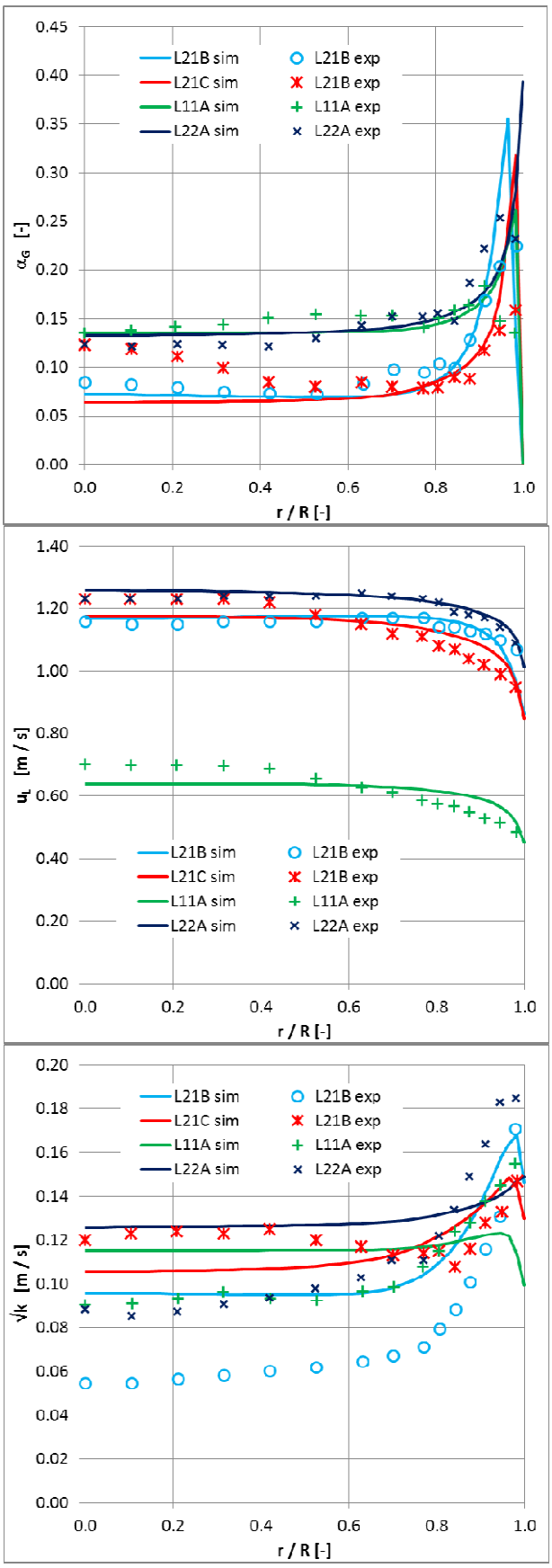

Figure 5: Gas volume fraction (top), axial liquid velocity (middle), and turbulent kinetic energy (bottom) for the tests of Liu (1998). Solid lines: simulation, symbols: experiment.

turbulent kinetic energy the agreement between simulation and measurement is not as good, but possibly to a large extent due to the isotropic approximation.

TOPFLOW tests

For the TOPFLOW test stationary axisymmetric simulations were done with the gas inlet modeled as individual nozzles. The pressure effect is included in the calculation using the MUSIG model since the implementation in CFX is based on classes of bubble mass and a transformation to / from bubble size occurs only as part of the pre- / post-processing. Two velocity groups were used as described above. For the size groups a width Δd_B = 1.0 mm was set and as many groups as needed to cover the range of the measured distributions from inlet to outlet were used.

Results for the development of gas volume fraction profiles are shown in Fig. 6. It can be seen that near the inlet the wall peak is underestimated by the simulation, but at the higher levels it is overpredicted. Likewise the initial width of the peak comes out too broad in the simulations, but the shoulder that develops subsequently has a narrower range than in the experiments.

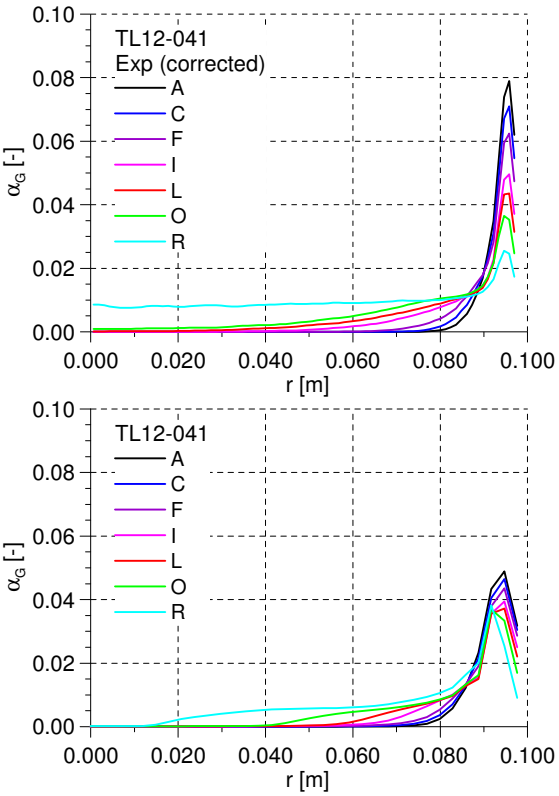

Figure 6: Gas volume fraction at different levels for the TOPFLOW test case TL12-041. Top: experimental data corrected as described in the text, bottom: simulation results.

CONCLUSION

A single model for bubbly two-phase flow has been applied to a range of diverse conditions. Reasonable agreement between data and simulations has been found for all investigated tests. Meaningful numbers quantifying the accuracy of the simulations are not readily given since experimental errors are rarely specified. As a rough guide it may be said that typical deviations between measured and simulated data are in the range of 15-20% for the void fraction and mean liquid velocity and 30-40% for the turbulent fluctuations. Maximum deviations tend to occur close to the wall where in the pipe flow cases the height of the void fraction peak is off by up to a factor of two whereas in the bubble column cases the point of zero liquid velocity is shifted which also results in a relative deviation up to a factor of two. This is encouraging for this first version of a baseline model although clearly there is still a need to expand its range of validated applicability as well as the quantitative agreement with the data.

To improve the model correlations for the bubble forces terms including effects of shear, turbulence and multiple bubbles should be derived from experiment of direct numerical simulations. The dependence of the turbulence source terms on additional dimensionless parameters like the ratio of bubble- and shear-induced length- and velocity scales could be obtained from direct numerical simulations as well.

REFERENCES

AUTON, T., HUNT, J. and PRUD'HOMME, M., (1988), "The force exerted on a body in inviscid unsteady non-uniform rotational flow", *J. Fluid Mech.,* **197**, 241.

BEYER, M., LUCAS, D., KUSIN, J. and SCHÜTZ, P., (2008), "Air-water experiments in a vertical DN200-pipe", *Helmholtz-Zentrum Dresden - Rossendorf* technical report FZD-505.

BURNS, A.D., FRANK, T., HAMILL, I. and SHI, J.-M., (2004), "The Favre averaged drag model for turbulence dispersion in Eulerian multi-phase flows", *5th Int. Conf. on Multiphase Flow*, ICMF2004, Yokohama, Japan.

DREW, D. A. and PASSMAN, S. L., (1998), "Theory of Multicomponent Fluids", *Springer*.

HOSOKAWA, S., TOMIYAMA, A., MISAKI, S. and HAMADA, T., (2002), "Lateral Migration of Single Bubbles Due to the Presence of Wall", *ASME Joint U.S.-European Fluids Engineering Division Conference*, FEDSM 2002, Montreal, Canada.

ISHII, M. and HIBIKI, T., (2011), "Thermo-fluid dynamics of two-phase flow", *Springer*, 2nd ed.

ISHII, M. and ZUBER, N., (1979), "Drag coefficient and relative velocity in bubbly, droplet or particulate flows", *AIChE J.,* **25**, 843.

KREPPER, E., LUCAS, D., FRANK, T., PRASSER, H.-M. and ZWART, P., (2008), "The inhomogeneous MUSIG model for the simulation of polydispersed flows", *Nucl. Eng. Des.,* **238**, 1690.

LIU, T. J., (1998), "The role of bubble size on liquid phase turbulent structure in two-phase bubbly flow", *3rd Int. Conf. on Multiphase Flow*, ICMF1998, Lyon, France.

LUCAS, D., BEYER, M., KUSSIN, J. and SCHÜTZ, P., (2010), "Benchmark database on the evolution of two-phase flows in a vertical pipe", *Nucl. Eng. Des.,* **240**, 2338.

LUCAS, D. and TOMIYAMA, A., (2011), "On the role of the lateral lift force in poly-dispersed bubbly flows", *Int. J. Multiphase Flow,* **37**, 1178.

MAGNAUDET, J., RIVERO, M. and FABRE, J., (1995), "Accelerated flows past a rigid sphere or a spherical bubble Part 1: Steady straining flow", *J. Fluid Mech.,* **284**, 97.

MAXEY, M. R. and RILEY, J. J., (1983), "Equation of motion for a small rigid sphere in a nonuniform flow", *Phys. Fluids,* **26**, 883.

MENTER, F.R. (2009). "Review of the shear-stress transport turbulence model experience from an industrial perspective", *Int. J. of Comput. Fluid Dyn.*, **23**, 305.

bin MOHD AKBAR, M.H., HAYASHI, K., HOSOKAWA, S. and TOMIYAMA, A., (2012), "Bubble tracking simulation of bubble-induced pseudo turbulence", *Multiphase Sci. Tech.*, **24**, 197.

MUDDE, R. F., HARTEVELD, W. K. and VAN DEN AKKER, H. E. A. (2009), "Uniform Flow in Bubble Columns", *Ind. Eng. Chem. Res.,* **48**, 148.

RZEHAK, R., KREPPER, E. and LIFANTE, C., (2012), "Comparative study of wall-force models for the simulation of bubbly flows", *Nucl. Eng. Des.,* **253**, 41.

RZEHAK, R. and KREPPER, E., (2013), "Closure Models for turbulent bubbly flows: A CFD study", *Nucl. Eng. Des.,* **265**, 701.

RZEHAK, R. and KREPPER, E., (2013a), "CFD modeling of bubble-induced turbulence", *Int. J. Multiphase Flow,* **55**, 138.

RZEHAK, R., LIAO, Y., LUCAS, D. and KREPPER, E., (2013), "Baseline model for CFD of dispersed bubbly flow", *15th International Topical Meeting on Nuclear Reactor Thermal-hydraulics*, NURETH-15, Pisa, Italy.

SCHMIDTKE, M., (2008), "Investigation of the dynamics of fluid particles using the Volume of Fluid Method", *University Paderborn*, PhD-Thesis (in German).

TOMIYAMA, A., SOU, A., ZUN, I., KANAMI, N. and SAKAGUCHI, (1995), "Effects of Eötvös number and dimensionless liquid volumetric flux on lateral motion of a bubble in a laminar duct flow", *2nd Int. Conf. on Multiphase Flow*, ICMF1995, Kyoto, Japan.

TOMIYAMA, A., KATAOKA, I., ZUN, I. and SAKAGUCHI, T., (1998), "Drag Coefficients of Single Bubbles under Normal and Micro Gravity Conditions", *JSME Int. J. B,* **41**, 472.

TOMIYAMA, A., TAMAI, H., ZUN, I. and HOSOKAWA, S., (2002), "Transverse migration of single bubbles in simple shear flows", *Chem. Eng. Sci.,* **57**, 1849.

WELLEK, R.M., AGRAWAL, A.K. and SKELLAND, A.H.P., (1966), "Shapes of liquid drops moving in liquid media", *AIChE J.,* **12**, 854.

WILCOX, D. C., (1998), "Turbulence Modeling for CFD", *DCW-Industries*.

YEOH, G. H. and TU, J. Y., (2010), "Computational Techniques for Multiphase Flows — Basics and Applications", *Butterworth-Heinemann*.

ZIEGENHEIN, T., LUCAS, D., RZEHAK, R. and KREPPER, E., (2013), "Closure relations for CFD simulation of bubble columns", *8th Int. Conf. on Multiphase Flow,* ICMF2013, Jeju, Korea.

ZUN, I., (1980), "The transverse migration of bubbles influenced by walls in vertical bubbly flow", *Int. J. Multiphase Flow,* **6**, 583.